Journal of Sound and Vibration (2002) **258**(2), 233–246
doi:10.1006/jsvi.5106, available online at http://www.idealibrary.com on IDEAL®

MODAL ANALYSIS OF ROTATING COMPOSITE CANTILEVER PLATES

H. H. Yoo

School of Mechanical Engineering, Hanyang University, Sungdong-Gu Haengdang-Dong 17, *Seoul* 133-791 *South Korea. E-mail: hhyoo@hanyang.ac.kr*

S. K. Kim

Triga Research Reactor D&D Team, Korea Atomic Energy Research Institute, Dukjin-Dong 150, *Yousung-Gu, Daejeon, South Korea. E-mail: sungkyun@ihanyang.ac.kr*

AND

D. J. Inman

Department of Mechanical Engineering, Center for Intelligent Material Systems and Structures, 310 *NEB, Mail Code* 0261, *Blacksburg, VA* 24061, *U.S.A. E-mail: dinman@vt.edu*

(*Received* 25 *September* 2001, *and in final form* 4 *March* 2002)

A modelling method for the modal analysis of a rotating composite cantilever plate is presented in this paper. A set of linear ordinary differential equations of motion for the plate is derived by using the assumed mode method. Two in-plane stretch variables are employed and approximated to derive the equations of motion. The equations of motion include the coupling terms between the in-plane and the lateral motions as well as the motion-induced stiffness variation terms. Dimensionless parameters are identified and the explicit mass and the stiffness matrices for the modal analysis are obtained with the dimensionless parameters. The effects of the dimensionless angular velocity and the fiber orientation angles of rotating composite cantilever plates on their modal characteristics are investigated. Natural frequency loci veering and crossing along with associated mode shape variations are observed.

1. INTRODUCTION

Composite structures, especially laminated composite plates, have been widely used in many engineering examples in aeronautical, astronautical, and marine structures. In addition to the advantages of high strength (as well as high stiffness) and light weight, another advantage of the laminated composite plate is the controllability of the structural properties through changing the fiber orientation angles and the number of plies and selecting proper composite materials.

While studies on laminated composite structures were actively progressed in the 1980s (see, for instance references [1–5]), flexible structures having slender shapes were often idealized as beams. Reliable and robust theories for beams, which can provide accurate numerical results in most cases, are available. Many structures, however, have plate-like shapes rather than beam-like shapes. Solar panels and solar sails of satellites, turbine blades, and aircraft rotary wings which have small aspect ratios are such examples. Obviously, these structures can be analyzed more accurately by modelling them as plates

0022-460X/02/$35.00

rather than beams. During the last three decades a few results for rotating cantilever plates have been presented (see references [6, 7]). These efforts employed finite element techniques and strain energy expressions which were obtained from equilibrium conditions between the centrifugal inertia forces and the steady state in-plane stress components. On the basis of this approach, the modal characteristics of rotating plates could be estimated by calculating explicit stiffness matrices. This approach, however, involves unnecessary assumptions and complexities which result in a two-step procedure to derive the equations of motion for rotating plates. These added complexities make it extremely difficult to apply this approach to practical problems. In addition, the Coriolis coupling effects between the in-plane and the lateral motions cannot be considered in this approach. Recently, a new modelling method, which employs a hybrid set of deformation variables for a plate, was introduced (see reference [8]). This modelling method is much simpler than the previous method in deriving the equations of motion and performing the numerical analysis. Moreover, the Coriolis coupling effects between the in-plane and the lateral motions can be considered. To date this modelling method has been applied to only isotropic plates. Here, the method is extended to composite plates. Since composite plates are used for many rotating structures nowadays, the method and the results obtained through this study can be used for the designs of the structures.

The purpose of this paper is to investigate the modal characteristics of rotating composite plates. The equations of motion are derived and transformed into dimensionless forms. Dimensionless parameters are identified and the effects of the dimensionless angular speed and the fiber orientation angles on the modal characteristics of rotating composite plates are investigated. The coupling effects between the in-plane and the bending motions are examined. In addition, natural frequency loci veering, loci crossing, and associated mode shape variations are observed and discussed. These have never been discussed in previous works.

2. EQUATIONS OF MOTION

Figure 1 shows a rotating rectangular plate which is characterized by natural length a, width b, and thickness h. The thickness of the plate is assumed to be uniform and small

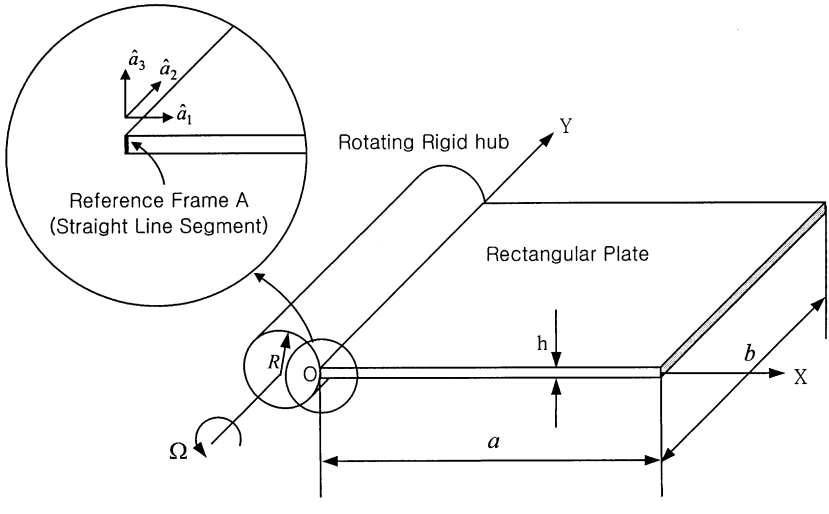

Figure 1. Configuration of a rotating rectangular plate.

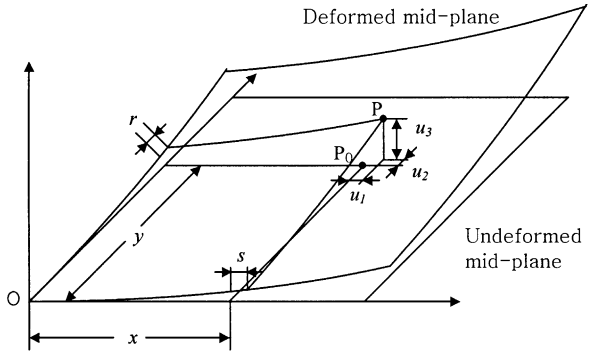

Figure 2. Deformation variables for a rectangular plate.

compared to other dimensions of the plate so that the Kirchhoff hypothesis can be employed. So the transverse shear and the rotary inertia effects are ignored in this study. This assumption is made to simplify the formulation in order to focus on the major issue of the present study, which is the stiffness variation due to the overall motion. The plate is attached to a rigid hub (of radius R) which rotates with a constant angular speed Ω.

By the Kirchhoff hypothesis, any straight line segments perpendicular to the mid-plane of the plate before deformation remain perpendicular to the mid-plane after deformation. Therefore, any one of them can be used as a rigid reference frame for the plate. In this study, the straight line segment at a corner of the rectangular plate (where point O is located) is used as the reference frame as shown in the figure. A unit vector triad ($\hat{a}_1$, $\hat{a}_2$, and $\hat{a}_3$) is fixed to the reference frame.

Figure 2 shows the mid-planes of a rectangular plate before and after deformation. The elastic deformation of a generic point in the mid-plane is denoted as $\mathbf{u}$ (the vector from point P_0 to point P shown in the figure). Three Cartesian variables (u_1, u_2, and u_3 as shown in the figure) are employed to express the elastic deformation vector. Conventionally, the three Cartesian deformation variables are approximated to obtain ordinary differential equations of motion. In the present study, however, u_1 and u_2 are not approximated while u_3 is approximated. Instead, two in-plane stretch variables (s and r shown in the figure) are approximated. Thus, by using the Rayleigh–Ritz method, they can be expressed as follows:

$$s(x,y,t) = \sum_{j=1}^{\mu} \phi_{1j}(x,y)q_j(t), \qquad r(x,y,t) = \sum_{j=1}^{\mu} \phi_{2j}(x,y)q_j(t),$$

$$u_3(x,y,t) = \sum_{j=1}^{\mu} \phi_{3j}(x,y)q_j(t), \tag{1,2,3}$$

where ϕ_{1j}, ϕ_{2j}, and ϕ_{3j} are spatial mode functions. Any compact set of admissible functions which satisfy the geometric boundary conditions of the plate can be used as the mode functions. The q_j's are generalized co-ordinates and μ is the total number of the generalized co-ordinates. For convenience of formalism, s, r, and u_3 use the same number of co-ordinates μ. However, they are not actually coupled. For instance, ϕ_{1j} is not zero only if $j \leqslant \mu_1$; ϕ_{2j} is not zero only if $\mu_1 < j \leqslant \mu_1 + \mu_2$; and ϕ_{3j} is not zero only if $\mu_1 + \mu_2 < j \leqslant \mu_1 + \mu_2 + \mu_3$. In other words, μ_1, μ_2, and μ_3 denote the actual numbers of generalized co-ordinates for s, r, and u_3 respectively. The scalar μ is the total sum of μ_1, μ_2, and μ_3.

The elastic strain energy of a composite plate can be expressed as follows (see reference [9]):

$$
\begin{aligned}
U = \frac{1}{2}\int_0^b \int_0^a \Bigg[& A_{11}\left(\frac{\partial s}{\partial x}\right)^2 + 2A_{12}\frac{\partial s}{\partial x}\frac{\partial r}{\partial y} + A_{22}\left(\frac{\partial r}{\partial y}\right)^2 \\
& + 2\left(A_{16}\frac{\partial s}{\partial x} + A_{26}\frac{\partial r}{\partial y}\right)\left(\frac{\partial s}{\partial y} + \frac{\partial r}{\partial x}\right) + A_{66}\left(\frac{\partial s}{\partial y} + \frac{\partial r}{\partial x}\right)^2 \\
& - 2B_{11}\frac{\partial s}{\partial x}\frac{\partial^2 u_3}{\partial x^2} - 2B_{12}\left(\frac{\partial r}{\partial y}\frac{\partial^2 u_3}{\partial x^2} + \frac{\partial s}{\partial x}\frac{\partial^2 u_3}{\partial y^2}\right) - 2B_{22}\frac{\partial r}{\partial y}\frac{\partial^2 u_3}{\partial y^2} \\
& - 2B_{16}\left[\frac{\partial^2 u_3}{\partial x^2}\left(\frac{\partial s}{\partial y} + \frac{\partial r}{\partial x}\right) + 2\frac{\partial s}{\partial x}\frac{\partial^2 u_3}{\partial x \partial y}\right] \\
& - 2B_{26}\left[\frac{\partial^2 u_3}{\partial y^2}\left(\frac{\partial s}{\partial y} + \frac{\partial r}{\partial x}\right) + 2\frac{\partial r}{\partial y}\frac{\partial^2 u_3}{\partial x \partial y}\right] - 4B_{66}\frac{\partial^2 u_3}{\partial x \partial y}\left(\frac{\partial s}{\partial y} + \frac{\partial r}{\partial x}\right) \\
& + D_{11}\left(\frac{\partial^2 u_3}{\partial x^2}\right)^2 + 2D_{12}\frac{\partial^2 u_3}{\partial x^2}\frac{\partial^2 u_3}{\partial y^2} + D_{22}\left(\frac{\partial^2 u_3}{\partial y^2}\right)^2 \\
& + 4\left(D_{16}\frac{\partial^2 u_3}{\partial x^2} + D_{26}\frac{\partial^2 u_3}{\partial y^2}\right)\frac{\partial^2 u_3}{\partial x \partial y} + 4D_{66}\left(\frac{\partial^2 u_3}{\partial x \partial y}\right)^2 \Bigg] \mathrm{d}x\,\mathrm{d}y,
\end{aligned} \tag{4}
$$

where matrices A_{ij}, B_{ij}, and D_{ij} can be obtained by integrating the material properties of each layer of a composite plate (as shown in Figure 3) as follows:

$$A_{ij} = \int_{-h/2}^{h/2} Q_{ij}^{(k)}\,\mathrm{d}z = \sum_{k=1}^{N} Q_{ij}^{(k)}(z_k - z_{k-1}), \tag{5}$$

$$B_{ij} = \int_{-h/2}^{h/2} Q_{ij}^{(k)} z\,\mathrm{d}z = \frac{1}{2}\sum_{k=1}^{N} Q_{ij}^{(k)}(z_k^2 - z_{k-1}^2), \tag{6}$$

$$D_{ij} = \int_{-h/2}^{h/2} Q_{ij}^{(k)} z^2\,\mathrm{d}z = \frac{1}{3}\sum_{k=1}^{N} Q_{ij}^{(k)}(z_k^3 - z_{k-1}^3), \tag{7}$$

where $Q_{ij}^{(k)}$ are the off-axis stiffness of kth layer, z_k and z_{k-1} are the distance from the mid-plane to the top and bottom surface of the kth layer, and N is the total number of laminated layers. The laminated plate geometry and ply numbering system is also shown in Figure 3 and the co-ordinates and fiber direction of kth-layer angle-ply laminated composite plate are shown in Figure 4.

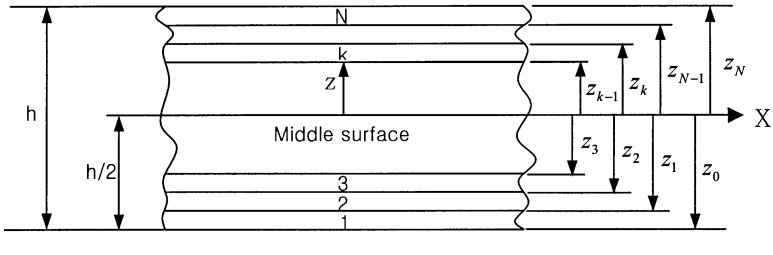

Figure 3. Laminated plate geometry and ply numbering system.

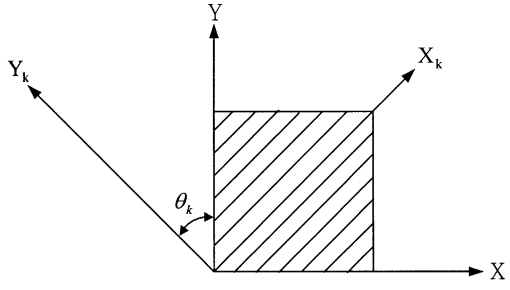

Figure 4. Fiber direction of the kth layer.

By using the strain energies given in equation (4), generalized active forces (see reference [10]) can be obtained as follows:

$$F_i = -\frac{\partial U}{\partial q_i} \quad (i = 1, 2, \ldots, \mu). \tag{8}$$

The use of s and r results in the advantage of obtaining the exact quadratic form of in-plane strain energy. Thus, exact linear generalized active forces can be obtained. Unfortunately, this complicates the formulation of generalized inertia forces in the equations of motion. Generalized inertia forces (see reference [10]) can be obtained by using the following equation:

$$F_i^* = -\int_0^b \int_0^a \rho \left(\frac{\partial \mathbf{v}^P}{\partial \dot{q}_i} \right) \cdot \mathbf{a}^P \, \mathrm{d}x \, \mathrm{d}y \quad (i = 1, 2, \ldots, \mu), \tag{9}$$

where ρ is the mass per unit area of the plate; $\dot{q}_i$'s are the time derivatives of the generalized co-ordinates; and $\mathbf{v}^P$ and $\mathbf{a}^P$ are the velocity and the acceleration of the generic point P. The velocity of point P can be obtained from the following equation:

$$\mathbf{v}^P = \mathbf{v}^O + \boldsymbol{\omega}^A \times (\mathbf{p} \times \mathbf{u}) + {}^A\mathbf{v}^P, \tag{10}$$

where $\mathbf{v}^O$ is the velocity of point O which is the reference point fixed in the rigid frame A; $\boldsymbol{\omega}^A$ is the angular velocity of the rigid frame A; $\mathbf{p}$ is the position vector from O to P_0; and ${}^A\mathbf{v}^P$ is the relative velocity P observed from the rigid frame A, which can be obtained by taking the time derivative of $\mathbf{u}$ in the rigid frame A. Here component notation, $\mathbf{v}^O$, $\boldsymbol{\omega}^A$, $\mathbf{p}$ and ${}^A\mathbf{v}^P$ defined by

$$\mathbf{v}^O = R\Omega\hat{\mathbf{a}}_3, \qquad \boldsymbol{\omega}^A = -\Omega\hat{\mathbf{a}}_2, \tag{11, 12}$$

$$\mathbf{p} = x\hat{\mathbf{a}}_1 + y\hat{\mathbf{a}}_2, \qquad {}^A\mathbf{v}^P = \dot{u}_1\hat{\mathbf{a}}_1 + \dot{u}_2\hat{\mathbf{a}}_2 + \dot{u}_3\hat{\mathbf{a}}_3 \tag{13, 14}$$

is used. By substituting equations (11)–(14) into Equation (10), the velocity of point P can be obtained as follows:

$$\mathbf{v}^P = [\dot{u}_1 - \Omega u_3]\hat{\mathbf{a}}_1 + [\dot{u}_2]\hat{\mathbf{a}}_2 + [\dot{u}_3 + \Omega(R + x + u_1)]\hat{\mathbf{a}}_3. \tag{15}$$

Since u_1, $\dot{u}_1$, and $\dot{u}_2$ shown in equation (15) are not approximated, they need to be replaced by using s, r, u_3, $\dot{s}$, $\dot{r}$, and $\dot{u}_3$. The geometric relations between the in-plane

stretch variables and the Cartesian deformation variables are given (see reference [11]) as follows:

$$x + s = \int_0^x \left[\left(1 + \frac{\partial u_1}{\partial \xi} \right)^2 + \left(\frac{\partial u_3}{\partial \xi} \right)^2 \right]^{1/2} \mathrm{d}\xi, \tag{16}$$

$$y + r = \int_0^y \left[\left(1 + \frac{\partial u_2}{\partial \eta} \right)^2 + \left(\frac{\partial u_3}{\partial \eta} \right)^2 \right]^{1/2} \mathrm{d}\eta. \tag{17}$$

Since linear equations of motion are to be derived eventually in the present study, up to second degree terms are to be retained to avoid premature linearization (see reference [10]) until the partial velocities are obtained. By using the binomial expansion theorem, the above two equations can be approximated as follows:

$$s = u_1 + \frac{1}{2} \int_0^x \left[\left(\frac{\partial u_3}{\partial \xi} \right)^2 \right] \mathrm{d}\xi, \tag{18}$$

$$r = u_2 + \frac{1}{2} \int_0^y \left[\left(\frac{\partial u_3}{\partial \eta} \right)^2 \right] \mathrm{d}\eta. \tag{19}$$

Differentiations of equations (18) and (19) with respect to time yield

$$\dot{s} = \dot{u}_1 + \int_0^x \left[\left(\frac{\partial \dot{u}_3}{\partial \xi} \right) \left(\frac{\partial u_3}{\partial \xi} \right) \right] \mathrm{d}\xi, \tag{20}$$

$$\dot{r} = \dot{u}_2 + \int_0^y \left[\left(\frac{\partial \dot{u}_3}{\partial \eta} \right) \left(\frac{\partial u_3}{\partial \eta} \right) \right] \mathrm{d}\eta. \tag{21}$$

Thus, $\dot{u}_1$ and $\dot{u}_2$ in equation (15) can be replaced by $\dot{s}$, $\dot{r}$, and $\dot{u}_3$. By using equations (20) and (21) along with equations (15) and (1)–(3), the partial derivative of $\mathbf{v}^P$ with respect to $\dot{q}_i$ can be obtained as follows:

$$\frac{\partial \mathbf{v}^P}{\partial \dot{q}_i} = \left[\phi_{1i} - \sum_{j=1}^{\mu} \int_0^x \phi_{3i,\xi} \phi_{3j,\xi} \, \mathrm{d}\xi q_j \right] \hat{\boldsymbol{a}}_1$$

$$+ \left[\phi_{2i} - \sum_{j=1}^{\mu} \int_0^y \phi_{3i,\eta} \phi_{3j,\eta} \, \mathrm{d}\eta q_j \right] \hat{\boldsymbol{a}}_2 + [\phi_{3i}] \hat{\boldsymbol{a}}_3. \tag{22}$$

Now, by simply differentiating the velocity shown in equation (15) with respect to time, the acceleration of point P can be obtained. Then, by substituting the acceleration and the partial velocities shown in equation (22) into equation (9), the generalized inertia forces can be obtained. Linearizing the generalized inertia forces and adding them by the generalized active forces, the linear equations of motion for rotating composite plates can be obtained. A more detailed procedure to obtain the equations of motion is given in reference [8].

It is useful to obtain the equations of motion in a dimensionless form. For the purpose, the following dimensionless variables, parameter, and functions are

introduced:

$$\tau \equiv \frac{t}{T}, \quad \xi \equiv \frac{x}{a}, \quad \eta \equiv \frac{y}{b}, \quad \vartheta_j \equiv \frac{q_j}{a},$$
$$\phi_i(x,y) \equiv \varphi_i(\xi,\eta), \quad \omega \equiv \frac{\Omega}{\Omega_r}, \quad \sigma \equiv \frac{R}{a},$$
$$A_{ij}^1 \equiv \frac{T^2}{\rho a^2}A_{ij}, \quad A_{ij}^2 \equiv \frac{T^2}{\rho ab}A_{ij}, \quad A_{ij}^3 \equiv \frac{T^2}{\rho b^2}A_{ij},$$
$$B_{ij}^1 \equiv \frac{T^2}{\rho a^3}B_{ij} \quad B_{ij}^2 \equiv \frac{T^2}{\rho ab^2}B_{ij}, \quad B_{ij}^3 \equiv \frac{T^2}{\rho a^2 b}B_{ij},$$
$$B_{ij}^4 \equiv \frac{T^2}{\rho b^3}B_{ij} \quad D_{ij}^1 \equiv \frac{T^2}{\rho a^4}D_{ij}, \quad D_{ij}^2 \equiv \frac{T^2}{\rho a^2 b^2}D_{ij},$$
$$D_{ij}^3 \equiv \frac{T^2}{\rho b^4}D_{ij} \quad D_{ij}^4 \equiv \frac{T^2}{\rho a^3 b}D_{ij}, \quad D_{ij}^5 \equiv \frac{T^2}{\rho ab^3}D_{ij}, \tag{23}$$

where Ω_r and T are defined as

$$\Omega_r \equiv \sqrt{\frac{D_{11}}{\rho a^4}}, \qquad T \equiv \frac{1}{\Omega_r}. \tag{24}$$

Using these dimensionless variables and parameters, the following linear dimensionless equations of motion for composite plate can be eventually derived:

$$\sum_{j=1}^{\mu}[M_{ij}^{11}\ddot{\vartheta}_j + (-\omega^2 M_{ij}^{11} + K_{ij}^{S1\,11,11} + K_{ij}^{S2\,11,12} + K_{ij}^{S2\,11,21} + K_{ij}^{S3\,11,22})\vartheta_j + (K_{ij}^{S2\,12,22} + K_{ij}^{S1\,12,12} + K_{ij}^{S3\,12,11} + K_{ij}^{S2\,12,21})\vartheta_j + 2\omega M_{ij}^{13}\dot{\vartheta}_j + (-K_{ij}^{C1\,1,111} - K_{ij}^{C2\,1,122} - K_{ij}^{C3\,1,211} - 2K_{ij}^{C3\,1,112} - K_{ij}^{C4\,1,222} - 2K_{ij}^{C2\,1,212})\vartheta_j] = 0, \tag{25}$$

$$\sum_{j=1}^{\mu}[M_{ij}^{22}\ddot{\vartheta}_j + (K_{ij}^{S3\,22,22} + K_{ij}^{S2\,22,21} + K_{ij}^{S2\,22,12} + K_{ij}^{S1\,22,11})\vartheta_j + (-K_{ij}^{C3\,2,211} - K_{ij}^{C4\,2,222} - K_{ij}^{C1\,2,111} - K_{ij}^{C2\,2,122} - 2K_{ij}^{C2\,2,212} - 2 - K_{ij}^{C2\,2,112})\vartheta_j + (K_{ij}^{S2\,21,21} + K_{ij}^{S1\,21,11} + K_{ij}^{S3\,21,22} + K_{ij}^{S2\,21,12})\vartheta_j] = 0, \tag{26}$$

$$\sum_{j=1}^{\mu}[M_{ij}^{33}\ddot{\vartheta}_j + (-\omega^2 M_{ij}^{33} + K_{ij}^{B1\,11,11} + K_{ij}^{B2\,11,22} + K_{ij}^{B2\,22,11} + K_{ij}^{B3\,22,22} + 2K_{ij}^{B4\,11,12} + 2K_{ij}^{B4\,12,11} + 2K_{ij}^{B5\,22,12} + 2K_{ij}^{B5\,12,22} + 4K_{ij}^{B2\,12,12} + \sigma\omega^2 K_{ij}^{GX1} + \omega^2 K_{ij}^{GX12})\vartheta_j + (-K_{ij}^{C1\,1,111} - K_{ij}^{C2\,1,122} - K_{ij}^{C3\,1,211} - 2K_{ij}^{C3\,1,121} - -K_{ij}^{C4\,1,122} - 2K_{ij}^{C2\,1,221})\vartheta_j + (-K_{ij}^{C3\,2,211} - K_{ij}^{C4\,2,222} - K_{ij}^{C1\,2,111} - K_{ij}^{C2\,2,122} - 2 - {}_{ij}^{C2\,2,221} - 2K_{ij}^{C3\,2,121})\vartheta_j - 2\omega M_{ij}^{31}\dot{\vartheta}_j] = 0, \tag{27}$$

where

$$M_{ij}^{kl} = \int_0^1 \int_0^1 \varphi_{ki}\varphi_{lj}\,\mathrm{d}\xi\,\mathrm{d}\eta, \tag{28}$$

$$K_{ij}^{S\alpha\,kl,mn} = A_{ij}^{\alpha} \int_0^1 \int_0^1 \varphi_{ki,\Gamma_m}\varphi_{lj,\Gamma_n}\,\mathrm{d}\xi\,\mathrm{d}\eta, \tag{29}$$

$$K_{ij}^{C\alpha\,kl,mn} = B_{ij}^{\alpha} \int_0^1 \int_0^1 \varphi_{ki,\Gamma_l}\varphi_{3j,\Gamma_m\Gamma_n}\,\mathrm{d}\xi\,\mathrm{d}\eta, \tag{30}$$

$$K_{ij}^{B\alpha\,kl,mn} = D_{ij}^{\alpha} \int_0^1 \int_0^1 \varphi_{3i,\Gamma_k\Gamma_l}\varphi_{3j,\Gamma_m\Gamma_n}\,\mathrm{d}\xi\,\mathrm{d}\eta, \tag{31}$$

$$K_{ij}^{GX1} = \int_0^1 \int_0^1 (1-\xi)\varphi_{3i,\xi}\varphi_{3j,\xi}\,\mathrm{d}\xi\,\mathrm{d}\eta, \tag{32}$$

$$K_{ij}^{GX2} = \int_0^1 \int_0^1 \frac{1}{2}(1-\xi^2)\varphi_{3i,\xi}\varphi_{3j,\xi}\,\mathrm{d}\xi\,\mathrm{d}\eta, \tag{33}$$

where a comma denotes partial differentiation with respect to subscripts that follow. If m is 1, Γ represents ξ and if m is 2, Γ represents η.

Using equations (25)–(27), the matrix form of the equations of motion can be derived as follows:

$$\mathbf{M}\ddot{\vartheta} + \mathbf{C}\dot{\vartheta} + \mathbf{K}\vartheta = 0, \tag{34}$$

where

$$\mathbf{M} = \begin{bmatrix} M_{ij}^{11} & 0 & 0 \\ 0 & M_{ij}^{2} & 0 \\ 0 & 0 & M_{ij}^{33} \end{bmatrix}, \qquad \mathbf{C} = \begin{bmatrix} 0 & 0 & 2\omega M_{ij}^{13} \\ 0 & 0 & 0 \\ -2\omega M_{ij}^{31} & 0 & 0 \end{bmatrix}, \tag{35, 36}$$

$$K = \begin{bmatrix} K_{11} & K_{12} & K_{13} \\ K_{21} & K_{22} & K_{23} \\ K_{31} & K_{32} & K_{33} \end{bmatrix}, \tag{37}$$

where $\mathbf{K}$ is the symmetric whose respective element matrices K_{ij} are defined as

$$\begin{aligned} K_{11} &= -\omega^2 M^{11} + K^{S1\,11,11} + K^{S2\,11,12} + K^{S3\,11,21} + K^{S3\,11,22}, \\ K_{12} = K_{21} &= K^{S2\,12,22} + K^{S1\,12,12} + K^{S3\,12,11} + K^{S2\,12,21}, \end{aligned} \tag{38}$$

$$\begin{aligned} K_{13} = K_{31} = &- K^{C1\,1,111} - K^{C2\,1,122} - K^{C3\,1,211} - 2K^{C3\,1,112} \\ &- 2K^{C4\,1,222} - 2K^{C2\,1,212}, \end{aligned} \tag{39}$$

$$K_{22} = K^{S3\,22,22} + K^{S2\,22,21} + K^{S2\,22,12} + K^{S1\,22,11},$$

$$\begin{aligned} K_{23} = K_{32} = &- K^{C3\,2,211} - K^{C4\,2,222} - K^{C1\,2,111} - K^{C2\,2,122} \\ &- 2K^{C2\,2,212} - 2K^{C3\,1,112}, \end{aligned} \tag{40}$$

$$K_{33} = -\omega^2 M^{33} + K^{B1\ 11,11} + K^{B2\ 11,12} + K^{B2\ 22,11} + K^{B3\ 22,22} + 2K^{B4\ 11,12} + 2K^{B4\ 12,11} + 2K^{B5\ 22,12} + 2K^{B5\ 12,22} + 4K^{B2\ 12,12} + \sigma\omega^2 K^{GX1} + \omega^2 K^{GX2}. \quad (41)$$

In order to use a complex modal analysis method, equation (34) is transformed into the following form:

$$\mathbf{M}^*\dot{\mathbf{Z}} + \mathbf{K}^*\mathbf{Z} = 0, \quad (42)$$

where

$$\mathbf{M}^* = \begin{bmatrix} \mathbf{M} & \mathbf{0} \\ \mathbf{0} & \mathbf{I} \end{bmatrix}, \qquad \mathbf{K}^* = \begin{bmatrix} \mathbf{C} & \mathbf{K} \\ -\mathbf{I} & \mathbf{0} \end{bmatrix}, \qquad Z = \begin{Bmatrix} \dot{\vartheta} \\ \vartheta \end{Bmatrix}. \quad (43-45)$$

An eigenvalue problem can be derived by assuming that $\mathbf{Z}$ is a harmonic matrix function of τ expressed as

$$Z = e^{\lambda\tau}\Theta, \quad (46)$$

where λ is the complex eigenvalue and Θ is the complex mode shape. Substituting equation (46) into equation (42) yields

$$\lambda\mathbf{M}^*\Theta + \mathbf{K}^*\Theta = 0. \quad (47)$$

Note that equation (47) is not a symmetric eigenvalue problem.

3. NUMERICAL RESULTS AND DISCUSSION

In this section, numerical results are obtained by using the modal equations which are derived in section 2. To solve the eigenvalues problem for the rotating composite plate, assumed mode functions are employed. Five cantilever beam functions and seven free–free beam functions which include two rigid body mode functions are employed to construct 35 plate mode functions (see reference [12] for more detailed procedure). The number of mode functions are sufficient to insure adequate convergence for the lowest six eigensolutions. To confirm the convergence and the accuracy, numerical results obtained by using the present modelling method are compared to those by using ANSYS for a non-rotating composite plate. The composite plate used in this example is made up of eight laminae with the fiber orientations [0, 45, −45, 90]s, and the composite material is T300/5208. The mechanical properties of the material are given in Table 1. It is shown in Table 2 that the lowest six natural frequencies of a square plate obtained by using the present modelling method agree well with those obtained by using ANSYS. To obtain the finite element solutions (ANSYS), 100 elements (element type is SHELL99) are employed to divide the plate evenly.

Figure 5 shows the variations of the lowest six dimensionless natural frequencies of a rotating square plate with fiber orientations [0, 45, −45, 90]s. The dimensionless hub

TABLE 1

Material properties of the composite plate

Material	E_1 (GPa)	E_2 (GPa)	G_{12} (GPa)	ν_{12}
T300/5208	181	10·3	7·17	0·28

TABLE 2

Comparison of natural frequencies of a square plate obtained by the present modelling and ANSYS

Mode	Present	ANSYS	Error (%)
1	1·0479	1·0422	0·55
2	1·9816	1·9567	1·27
3	4·6503	4·5453	2·31
4	6·6018	6·5249	1·18
5	8·0411	7·8710	2·16
6	10·0365	9·7834	2·58

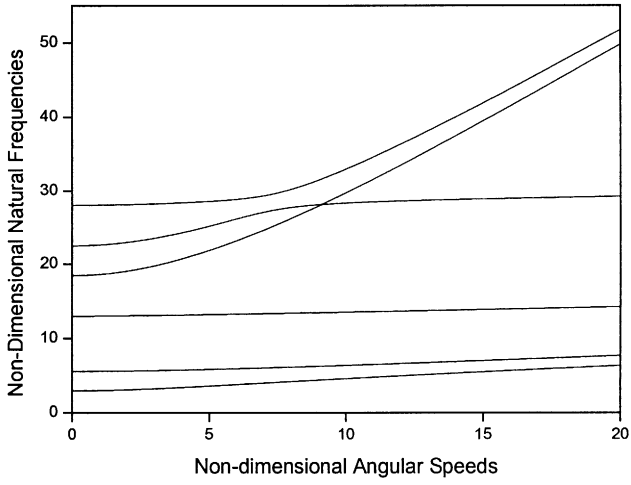

Figure 5. Variations of the lowest six natural frequencies of a rotating square composite plate.

radius ratio σ is set to zero. It can be observed from the results that all the natural frequencies increase as the angular speed increases. Interesting phenomena can be observed from Figure 5. The fifth and the sixth eigenvalue loci veer around $\omega = 7$ while the fourth and fifth eigenvalue loci cross around $\omega = 9$.

Figures 6(a) and 6(b) show the nodal lines of the lowest six modes of the plate when the dimensionless angular speeds are 0 and 20. Comparing the mode shapes of the rotating plate to those of the non-rotating plate, the fourth, the fifth, and the sixth mode shapes seem to be switched with one another. These mode shape variations result from the eigenvalue loci veering and crossing shown in Figure 5. These phenomena were well explained in reference [13]. Although the laminates of the plate are symmetrically stacked up with respect to neutral axis, nodal line patterns are found to be unsymmetric. The reason for this comes from the D_{16} and D_{26} terms which represent the flexural–torsional coupling effect in the matrix D_{ij} of equation (7). This same phenomenon was also reported in reference [14]. The flexural–torsional coupling effects, however, seem to be weakened as the angular speed of the plate increases. In this case, as the angular speed increases, the motion-induced stiffness variation terms of K^{GX1} and K^{GX2} become dominant so that the structural stiffness terms of D_{16} and D_{26} become negligible.

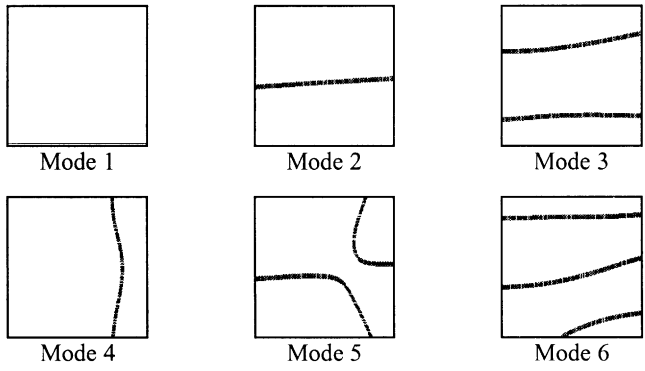

(a) Nodal lines of the lowest six modes without angular speed (ω=0)

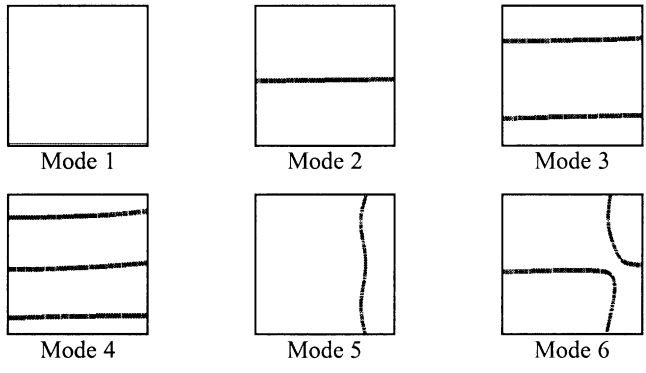

(b) Nodal lines of the lowest six modes with angular speed (ω=20)

Figure 6. Nodal line variations of the lowest six modes due to angular speed.

In Figure 7, the influence of the coupling effect between the in-plane and the lateral motions on the natural frequencies is investigated. The solid lines represent the results of considering the coupling effect and the dotted lines represent the results of ignoring the effect. When laminates are symmetrically staked up with respect to the neutral axis of the plate, the results obtained by considering the coupling effect are almost identical to those obtained by ignoring the coupling effect (as shown in Figure 7(a)). On the other hand, Figure 7(b) shows the variations of the lowest six dimensionless natural frequencies of a rotating plate with unsymmetrical fiber orientations [10, 20, 30, 40, 50, 60, 70, 80]. the results obtained by ignoring the coupling effect. In this case, B_{ij} which represents the coupling stiffness matrix in equation (6) is not zero and influences the modal characteristics of the rotating plate.

Lastly, the variations of dimensionless natural frequencies of a square plate for the fiber orientations [0, θ, $-\theta$, 90]s are shown in Figure 8. The effect of the fiber orientation angle θ is shown in the figure. Comparing Figures 8(a) and 8(b), one can find that the trends of the first bending, the first torsion, and the first chordwise bending frequencies are not much influenced by the angular speed while those of the second frequencies change significantly. These figures also indicate that the natural frequencies of the bending modes decrease as

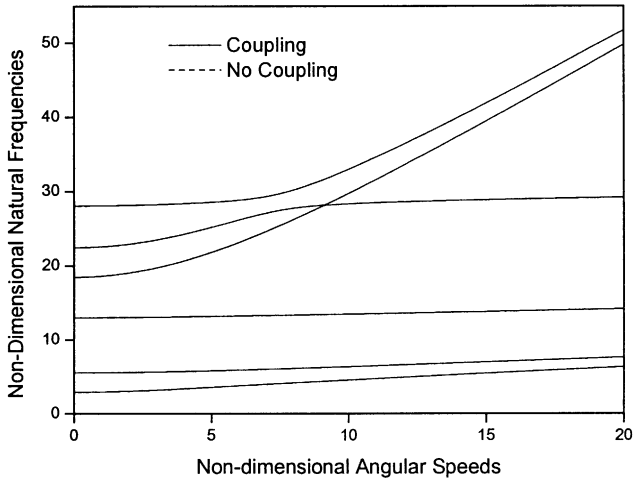

(a) Fiber orientation [0,45,-45,90]s

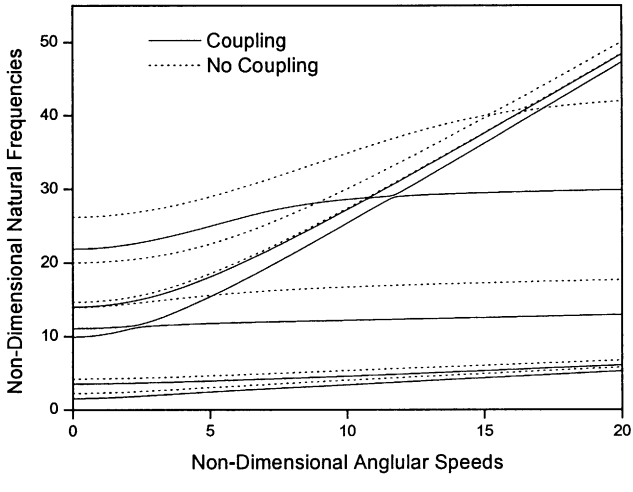

(b) Fiber orientation [10,20,30,40,50,60,70,80]

Figure 7. Variations of the lowest six natural frequencies of rotating composite plates with symmetrical and unsymmetrical laminae.

the fiber orientation angle increases. Those of the chordwise bending modes, however, increase as the fiber orientation angle increase.

4. CONCLUSIONS

In this paper, a modelling method for the modal analysis of rotating composite plates is presented. Using the proposed modelling method, the effects of the angular speed and the fiber orientation angles on the modal characteristics are investigated. As the angular speed increases, the natural frequencies increase. the natural frequency loci veering and the loci crossing phenomena are also observed from the numerical results. Mode shape variations which occur in the region of the veering and the crossing are also exhibited. When

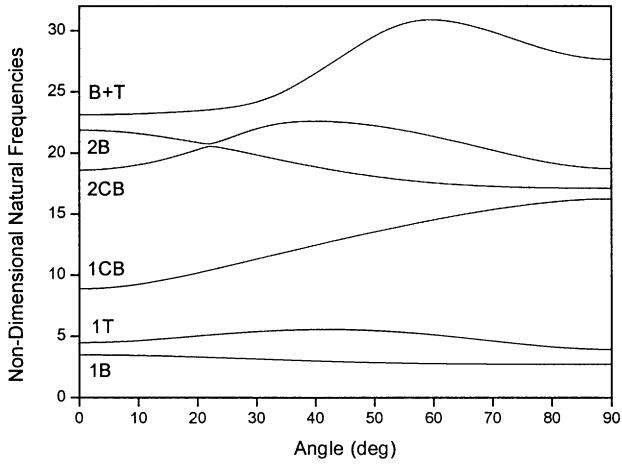

(a) $\omega = 0$

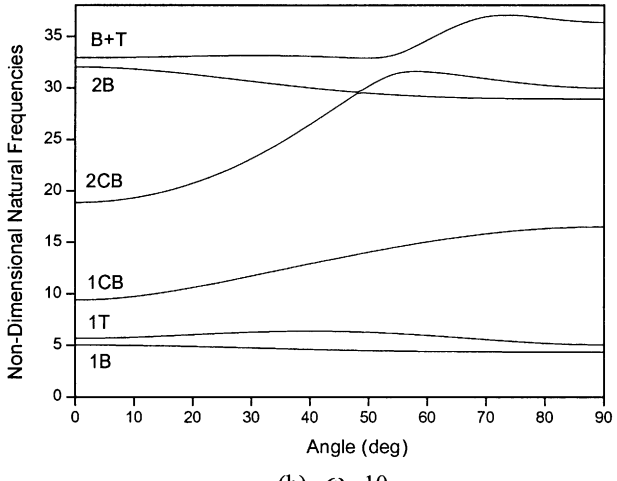

(b) $\omega = 10$

Figure 8. Variations of the lowest six natural frequencies due to the fiber orientation angle change.

laminates are unsymmetrically stacked up with respect to the mid-plane of the plate, the coupling effects between the in-plane and the lateral motions should be considered to obtain accurate analysis results. These results indicate that the modal characteristics of a rotating composite plate can be controlled by changing its fiber orientation angles.

ACKNOWLEDGMENTS

This research was supported by Center of Innovative Design Optimization Technology (iDOT), Korea Science and Engineering Foundation.

REFERENCES

1. R. Kapania and S. Raciti 1989 *American Institute of Aeronautics and Astronautics Journal* **27**, 201–210. Nonlinear vibrations of unsymmetrically laminated beams.

2. O. Rand 1991 *Journal of the American Helicopter Society* **36**, 3–11. Periodic response of thin-walled composite helicopter rotor blades.
3. S. Mohamed Nabi and N. Ganesan 1994 *Computers & Structures* **51**, 607–610. A generalized element of the free vibration analysis of composite beams.
4. H. Cudney and D. Inman 1989 *International Journal of Analytical and Experimental Modal Analysis* **4**, 138–143. Determining damping mechanisms in a composite beam.
5. K. Chandrashekhara, K. Krishnamurthy and S. Roy 1990 *Composite Structures* **14**, 269–279. Free vibration of composite beams including rotary inertia and shear deformation.
6. M. Dokainish and S. Rawtani 1971 *International Journal for Numerical Methods in Engineering* **3**, 233–248. Vibration analysis of rotating cantilever plates.
7. V. Ramamurti and R. Kielb 1984 *Journal of Sound and Vibration* **239**, 123–137. Dynamics of rectangular plates undergoing prescribed overall motion.
9. J. Whitney 1987 *Structural Analysis of Laminated Anisotropic Plates*. Pennsylvania: Technomic Publishing Co. Inc.
10. T. Kane and D. Levinson 1985 *Dynamics: Theory and Applications*. New York: McGraw-Hill Book Company.
11. L. Eisenhart 1964 *An Introduction to Differential Geometry*. Princeton: Princeton University Press.
12. A. Leissa 1969 *NASA SP*-160. Vibration of Plates.
13. A. Leissa 1974 *Journal of Applied Mathematics for Physics (ZAMP)* **25**, 99–111. On a curve veering aberration.
14. T. Maeda, V. Baburaj, Y. Ito and T. Koga 1998 *Journal of Sound and Vibration* **210**, 351–365. Flexural–torsional coupling effect on vibration characteristics of angle-ply laminates.